Journal of Applied Research and Technology

www.jart.icat.unam.mx
Journal of Applied Research and Technology 17 (2019) 203-212

Original

CoMoW/Al_2O_3-MgO-Li_2O Catalytic formulations for DBT hydrodesulphurization

D. A. Solis-Casados[a,*], J. Blancas-Blancas[a], L. Escobar-Alarcón[b], J. Escobar-Aguilar[c], T. Klimova[d], F. Gonzalez-Zavala[e]

[a]*Universidad Autónoma del Estado de México, Centro Conjunto de Investigación en Química Sustentable, UAEM-UNAM, km 14.5, Carretera Toluca-Atlacomulco, San Cayetano, Toluca Estado de México C.P. 50200, México.*
[b]*Departamento de Física, Instituto Nacional de Investigaciones Nucleares, Apdo. Postal 18-1027, 11801 México City, México*
[c]*Instituto Mexicano del Petróleo, Eje Central Lázaro Cárdenas 152, San Bartolo Atepehuacan, G.A. Madero, Cd. de México, 07730, México*
[d]*Facultad de Química, Departamento de Ingeniería Química, UNAM, México*
[e]*Universidad Autónoma Metropolitana Iztapalapa. Departamento de Física, Apdo. Postal 55-534, México City, México*

Abstract: Low acidity catalytic formulations were prepared incorporating MgO and Li_2O to the conventional CoMoW/Al_2O_3 catalysts. The CoMoW active phases were impregnated using an ammoniacal solution containing the metallic complexes as citrates. A high dispersion of the Co, Mo and W species in octahedral coordination, inhibiting the agglomeration towards phases like MoO_3, WO_3 and Co_3O_4, was attained. The obtained formulations preserve the catalytic activity in the hydrodesulphurization (HDS) reaction of dibenzothiophene (DBT), enhancing the selectivity towards the direct desulphurization route. The prepared formulations show a lower hydrogenation function due to its low acidity.

Keywords: selective HDS, DBT, low acidity formulations, CoMoW catalysts

1. INTRODUCTION

In the last few years, refining industry use for sulphur removal the hydrodesulphurization process (HDS), reacting in a lab scale with model molecules such as dibenzothiophene (DBT) and 4,6 dimethyldibenzothiophene (4,6-DMDBT), which are representatives of diesel and gasoils fuels (Ding, Zhou, Wei, Jiang, & Zhou, 2018; Wang, Wang, & Yu, 2012). Sulphur removal has been carried out through two main reaction routes, in one hand the hydrodesulphurization (HDS) where sulphur is removed by the molecule hydrogenation (HYD) and in the other hand the direct desulphurization (DDS) where sulphur is removed by the cleavage of the C-S bond, this side-reaction takes place with a reaction rate slower than the hydrogenation side-reaction. Catalysts used commonly for this HDS reaction are based on Ni(Co) Mo (W) sulphides supported on alumina, that have high acidity and are able to remove the sulphur from the DBT molecules by the hydrogenation route (Klicpera & Zdražil, 2002). In the past has been

* Corresponding author.
E-mail address: solis_casados@yahoo.com.mx (D. A. Solis-Casados)
Peer Review under the responsibility of Universidad Nacional Autónoma de México.

reported the same active phases in different catalytic supports, such as SiO_2, TiO_2, SiO_2-Al_2O_3, MCM-41, SBA-15 to cite some of them, although the HDS activity has been increased, the direct desulphurization has been inhibited (Ganiyu, Ali, & Alhooshani, 2017; Gómez-Orozco et al., 2018; Halachev, Atanasova, Agudo, Arias, & Ramirez, 2019; Huirache-Acuña et al., 2006; Nikulshina et al 2019; Kwak, Lee, Bae, Choi, & Moon, 2000; Obeso-Estrella et al., 2018). It is important to remark that in most cases nature of the catalytic support is acidic; in very few cases, catalytic formulations with low acidity have been reported for the sulphur elimination, with low hydrogenation of the DBT molecules. However, these have the inconvenient of the decrease in their catalytic activity. This leads to the proposal of incorporate tungsten as an active phase to keep the catalytic activity showed by conventional $CoMo/Al_2O_3$ formulations decreasing the hydrogenation function at the same time (Payen, Hubaut, Kasztelan, Poulet, & Grimblot, 1994). In this work, it is investigated the effect of incorporate Mg and Li into the conventional CoMoW catalytic formulation (Escobar-Alarcón et al., 2013). $CoMoW/Al_2O_3$-MgO and $CoMoW/Al_2O_3$ formulations were used as reference. Catalytic tests were performed through the HDS reaction of the DBT molecule, characteristic of some fuel fractions. It is expected that the $CoMoW/Al_2O_3$-MgO-Li_2O formulation preserve the catalytic activity enhancing the selectivity towards direct desulphurization, through a low hydrogenation function, which will result in the preservation of the octane number in fuels (Klimova, Casados, & Ramírez, 1998; Solís-Casados, Escobar, Orozco, & Klimova, 2010, Solís-Casados et al., 2016).

2. MATERIALS AND METHODS

2.1 PREPARATION OF CATALYTIC SUPPORTS

Catalytic supports were prepared following the procedure reported in a previous work (Solís-Casados et al., 2016). The chemical precursors were $Mg(OC_2H_5)_2$ (magnesium ethoxide Sigma, ACS reagent), AlOOH (pseudo-boehmite Catapal B TM Sassol), a solution of HCOOH 5 vol% (formic acid Sigma, ACS reagent, ≥96.0%), $C_6H_8O_7$ (citric acid Aldrich, ACS reagent, ≥ 99.5%) and LiOH (lithium hydroxide, Sigma–Aldrich, ACS reagent). Gelification of AlOOH was made by adding the solution of formic acid (HCOOH, 5 vol.%), this gel was used as a binder to conform pellets of the Al_2O_3 and Al_2O_3-MgO powders. The Al_2O_3-MgO pellets were impregnated with a solution of lithium hydroxide (LiOH) to produce the Al_2O_3-MgO-Li_2O support. All catalytic supports, Al_2O_3, Al_2O_3-MgO and Al_2O_3-MgO-Li_2O were obtained as pellets and were subjected to a thermal treatment at 500 °C for 4 h in an oven with air convection.

2.2 PREPARATION OF CATALYTIC FORMULATION

The catalytic supports in pellet form were impregnated by the incipient wet method using an ammoniacal solution containing citrates of Co, Mo and W, as complexes. The impregnant solution was prepared at 80 °C using an optimized method reported elsewhere (Ganiyu et al., 2017; Huirache-Acuña et al., 2006) with $CoCO_3$ monohydrated (Aldrich, 99.998 % trace metals basis), MoO_3 (Fermont) and $(NH_4)_6H_2W_{12}O_{40}$ xH_2O were used as metallic precursors. Citric acid ($C_6H_8O_7$, Aldrich) and NH_3 aqueous ammonia (Fermont) were used to stabilize the pH of the impregnant solution at 8.5 (Rimaldi et al., 2010). Impregnating solution was synthesized to get after impregnation and thermal treatment 12% MoO_3 and ratios of [Co/Co+ (Mo o W)] = 0.4 approximately. Once the supports were impregnated they were aged by 12 h until total dry. Finally, the impregnated supports were subjected to a thermal treatment at 400 ° C during 3 h in an oven air convection to obtain the catalyst precursors in their oxidized form.

2.3 SUPPORTS AND CATALYST CHARACTERIZATION

2.3.1 Chemical composition

CoMoW catalysts supported on Al_2O_3, Al_2O_3-MgO and Al_2O_3-MgO-Li_2O were characterized in the oxidized state, determining their elemental chemical composition. X-ray photoelectron spectroscopy (XPS) using a JEOL JPS 9200 XPS was employed to determine the elemental content in each sample. Wide and narrow spectra were acquired using a Mg Kα X-ray source with a pass energy of 30 eV, dwell 200 and 10 scans. Base line sustraction was done with the integral background of the Shirley-type model. Charge correction was required to interpret the true chemical shift, as an energy reference was used the adventitious carbon by setting the binding energy of C 1s to 285 eV. From photoelectron spectra were quantified the atomic elemental composition for each sample using the Specsurf software and their relative sensitivity factors, derived empirically and valid for the JEOL JPS 9200 spectrometer.

2.3.2 Acidity determination

Ammonia TPD experiments were carried out in a vacuum TPD system. The experiment of NH_3 thermodesorption was made by adsorbing the NH_3 adsorbate gas on the catalytic material. The adsorbent material was previously thermally treated (250 °C) in vacuum to remove the physisorbed water or weakly physisorbed CO_2. After NH_3 adsorption, samples were heated under an inert gas flow to remove the physisorbed NH_3 species. The outlet gas was monitored on-line with a temperature conductivity detector (TCD), converting the obtained signal to concentration units through a calibration curve.

2.3.3 Textural properties

Textural properties were measured by N_2-physisorption technique using an ASAP 2020 equipment from Micromeritics. The surface areas were calculated using the Brunnauer–Emmet–Teller (BET) equation. The adsorption–desorption isotherms were used to determine size (Kelvin equation) and shape of the pores. The total pore volume was measured at relative pressure ($P/P\circ$) equal to 0.99. All samples were degassed out at 250°C during 3 h (5 µm de Hg) previous to N_2-physisorption analysis.

2.3.4 Structural characterization

Infrared spectroscopy was used to corroborate the elimination of organic compounds. In order to determine crystalline phases present in the oxidized catalysts, X-ray powder diffraction (XRD) was carried out in a Bruker D8 Advance diffractometer equipped with a Linxeye detector, using Ni-filtered Cu Kα radiation. The measurement conditions were: 2 range = 5–80°, 22 step = 0.021°, acquisition time = 2.5 s per step. MicroRaman Spectroscopy was used to study the microstructural characteristics of the catalysts, this was done using an HR LabRam800 system equipped with an Olympus BX40 confocal microscope. A Nd:YAG laser beam (532 nm) was focused by a 50× microscope objective on to ≈1 µm diameter on the sample surface. The laser power at the sample was regulated by a neutral density filter (OD = 1) to prevent sample heating and structural changes induced in the sample. A CCD camera was used to record the the spectra, usually averaged for 100 accumulations in order to improve the signal to noise ratio. All spectra were calibrated using the 521 cm^{-1} line of a silicon wafer. Chemical coordination state and electronic transitions in catalysts as powders were determined from UV–Vis measurements. The spectra were recorded in the wavelength range from 200 to 1100 nm in the reflectance mode using a Perkin Elmer lambda-35 spectrophotometer equipped with a diffuse reflectance sphere with polytetrafluoroethylene as reference. Band gap energy was determined using the ultraviolet diffuse reflectance spectra. The band gap energy values can be related following an empirical procedure with the particle aggregation as was reported before (Weber, 1995).

2.3.5 Catalytic tests

The catalytic activity of the CoMoW catalysts supported onto Al_2O_3, Al_2O_3-MgO and Al_2O_3-MgO-Li(x) was tested in a pressurized batch reactor in the hydrodesulfurization of dibenzothiophene. Oxidized formulations were sulfided at 400°C (2 h) under an H_2S/H_2 (10%, v/v, Praxair) stream at a constant flow rate of 4 L/h. HDS activity was studied in a three-phase slurry batch reactor, Parr 4562 M. The mixture used in the reaction was prepared dissolving 300 mg of DBT in 100 ml of n-hexadecane as a solvent (both from Aldrich) and adding 200 mg of sieved catalyst (80–100 Tyler mesh, 0.165 mm of average particle diameter). The operation conditions were carefully chosen to avoid the external and/or internal diffusion limitations, were hydrogen pressure, P_{H2} was about 5.59 MPa, T = 260 and 320°C, working at 1000 rpm of mixing speed. Aliquots were taken each hour through the reaction time and analyzed in a gas chromatograph Perkin Elmer Auto System XL equipped with a flame ionization detector and Econopac-5 capillary column (Altech). The obtained products from the main reaction routes as direct desulfurization (DDS) and hydrogenation (HYD) were biphenyl (BP), cyclohexylbenzene (CHB) and diciclohexyl (DCH). The amount of these products at reaction times was followed by the gas chromatography analysis.

3. RESULTS AND DISCUSSION

3.1 CHARACTERIZATION OF OXIDIZED CATALYSTS

X-ray photoelectron spectroscopy data showing the atomic composition are shown in table 1. It is seen the presence of Mg and Li in the corresponding catalysts in amounts close to 5 % at. In general terms the composition data seem to be congruent to the theoretical expected. Also was expected that the addition of Mg and Li increases basic sites and consequently decrease the acidity in the concentration of acid sites as in their strength. This was measured by the total decrease in the concentration of NH_3 desorbed, indicating a decrease of the number of acidic sites. Table 2 shows the NH_3 concentration thermodesorbed at three different intervals of temperature corresponding with sites of different strength. The interval from 120 to 200 °C can be associated with weak strength sites (sites W); from 200 to 400 °C can be related with medium strength sites and from 400 to 500 °C correspond to strong strength sites. It is clearly seen that incorporation of MgO decreases approximately by 28.5% the total concentration of acidic sites whereas the simultaneous incorporation of MgO and Li_2O diminish almost 56.8 % the total concentration of acidic sites. The acidic strength considered as the ratio of the concentration of sites S to the concentration of sites M, decrease from 0.12 for Al_2O_3, to 0.06 and 0.05 for the catalysts supported on Al_2O_3-MgO and Al_2O_3-MgO-Li_2O, which represents a decrease of 50% and 58 % of acidic strength respectively. It is important to remark that the number of acidic sites and their strength will change the dispersion of precursors of active phases, it is probably that will be more agglomerated species in the catalysts supported on Al_2O_3 than in the other catalysts.

Table 1. Nominal composition determined by XPS.

% At	Theoretical CoMoW	CoMoW/ Al_2O_3	CoMoW/ Al_2O_3-MgO	CoMoW/ Al_2O_3-MgO-Li_2O
Co	0.6	1.0	1.1	0.7
Mo	1.0	0.8	0.8	0.3
W	1.0	1.5	2.0	0.3
Al	-	27.2	9.9	15.7
Mg	-		15.1	6.7
Li	-			28.4
O	-	69.4	71.2	49.9

Table 2. Concentration of NH_3 thermodesorbed, µmol/g.

Catalyst CoMoW/	Sites W 120-200 °C	Sites M 200-400 °C	Sites S 400-500 °C	Total	Acidic strength Sites S/Sites M
Al_2O_3	165.9	298.0	36.0	499.8	0.12
Al_2O_3-MgO	139.6	204.2	13.6	357.4	0.06
Al_2O_3-MgO-Li_2O	102.0	107.7	5.9	215.7	0.05

The incorporation of MgO and Li_2O to the catalytic support change the textural properties. The specific surface area determined by the BET equation reveal a decrease from 213 to 202 m^2/g when MgO is added to the Al_2O_3 support. On the other side incorporation of MgO and Li_2O to the support diminish the surface area to 179 m^2/g, as is observed in table 3. Specific surface area decreases in 5 % with MgO incorporation and decreases in 16 % after Li_2O incorporation to the catalytic formulation as was expected since MgO and Li_2O pure have low specific surface areas around 130 and 50 m^2/g. Both oxides MgO and Li_2O were incorporated with the purpose of decrease the number of acid sites and their acidic strength in catalytic formulation. Additionally, as it can be seen in table 3, the total pore volume remains almost the same, close to 0.11 cm^3/g, however, the mean pore diameter increases from 59 to 105 Å. These results can be attributed to the decrease in specific surface area with MgO and Li_2O incorporation to the catalytic formulation. In fact, figure 1 shows a broad distribution of the mean pore diameter. Figure 2 shows IV-type adsorption isotherms according to the IUPAC classification, which is indicative of mesoporous materials. The hysteresis shape suggests a bottle-neck type pore form.

Table 3. Textural properties of CoMoW catalyst.

Catalyst CoMoW/	Specific Surface area, BET (m^2/g)	Total pore volumen, BJH (cm^3/g)	Mean pore diameter (Å)
Al_2O_3	213	0.11	59
Al_2O_3-MgO	202	0.10	59
Al_2O_3-MgO-Li_2O	179	0.11	105

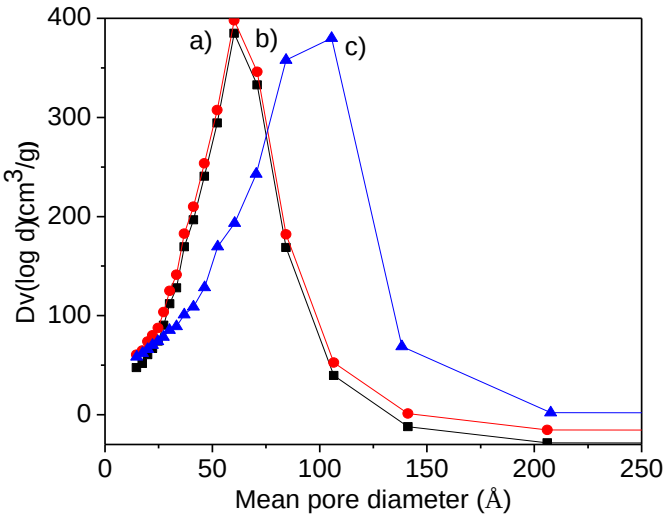

Fig. 1. Pore size distribution for a) CoMoW/Al_2O_3, b) CoMoW/Al_2O_3-MgO and c) CoMoW/ Al_2O_3-MgO-Li_2O

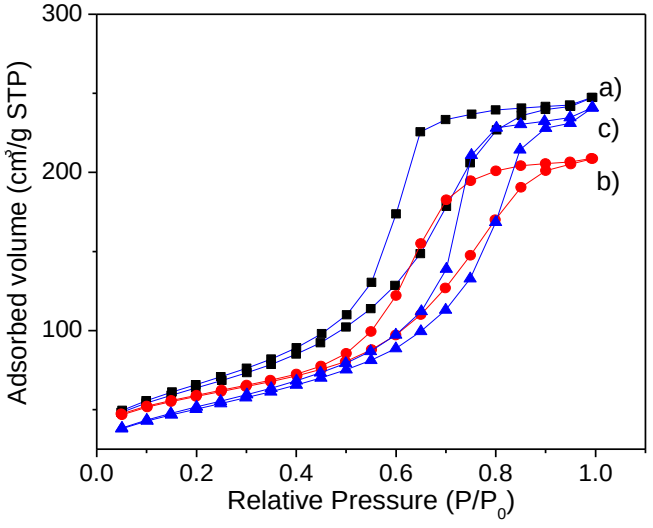

Fig. 2. N_2-physisorption Isotherms for a) CoMoW/Al_2O_3, b) CoMoW/Al_2O_3-MgO and c) CoMoW/ Al_2O_3-MgO-Li_2O catalysts.

In figure 3a) the diffraction patterns of the prepared samples are shown. Three main diffraction lines at 36.8, 45.9 and 66.7 ° associated to the γ-Al_2O_3 (JCPDS 01-074-2206) are observed. When MgO is incorporated to the support, these diffraction lines show a slight shift and broadening of the present peaks as figure 3b) reveals. Such changes could be attributed to the formation of a small proportion of the $Al_{2.408}Mg_{0.38}O_4$ crystalline phase (JCPDS 00-048-0528) coexisting with the alumina phase. In the CoMoW/ Al_2O_3-MgO-Li_2O formulation additional diffraction lines are observed at 19.9, 26.3, 26.4, 26.7º, which are attributed to the crystalline phase $Li_2Mg_2(WO_4)_3$ (JCPDS 01-082-1804). No diffraction signals associated with crystalline phases related to MoO_3, WO_3 and Co_3O_4 were observed. This can be explained in terms of the dispersion and low agglomeration of the CoMoW species in the prepared catalysts, as well as to crystallite sizes expected (lower than 40 Å) and also due to a dilution effect because of the low atomic concentration. Figure 4. I) shows Raman spectra of the CoMoW catalysts supported on Al_2O_3, Al_2O_3-MgO and Al_2O_3-MgO-Li_2O. Raman spectra are characterized by signals between 750-1000 cm^{-1}, as well as a band of less intensity around 320 cm^{-1} as can be seen in figure 4. I). The high frequency band peaking close to 950 cm^{-1}, can be attributed to several W and Mo species, in particular, the signal at 951 cm^{-1} can be assigned to the $Mo_7O_{24}^{6-}$ species, whereas the signal at approximately 836 cm^{-1} can be attributed to the asymmetric mode of stretching Mo-O-Mo bonds of molybdate species with octahedral coordination, the weak signal at 750 cm^{-1} corresponds to the symmetric O-W-O bonding (Clark, & Hester, 1987; Escobar-Alarcón et al., 2013; Klimova et al., 1998; Solís-Casados et al., 2010, 2016). It is important to note that signals attributed to the MoO_3, WO_3 and Co_3O_4 observed in figure 4.II) are absent in the prepared catalytic formulations; this is an argument to assume that species catalytically active are well dispersed on the surface of the support. After deconvolution of Raman spectra, it is clear that in all simples can be seen the band located at 749 cm^{-1} attributed to the O-W-O symmetric stretching. This Raman spectra were deconvoluted analyzing the broad band in the region of 800-1000 cm^{-1}, to corroborate the idea of the change of species as an effect of the support, where tetrahedral/octahedral ratio is increasing with lithium incorporation as was reported before (Solís-Casados et al., 2016; Pérez-Martínez, Eloy, Gaigneaux, Giraldo, & Centeno, 2010; Vakros, Lycourghiotis, Voyiatzis, Siokou, & Kordulis, 2010). The broad band between 800-1000cm^{-1} region is attributed mainly to the asymmetric stretching Mo=O bondings; however, this broad band was deconvoluted defining three main peaks in all spectra; it can be seen a shoulder located at 847-867 cm^{-1} which is characteristic of the asymmetric stretching of Mo-O-Mo species; in the 924-937 cm^{-1} region appear a band associated to the distorted tetrahedral Mo species, band that remains in all catalysts. The band located at 954 in catalyst supported on Al_2O_3 and 964 cm^{-1} in catalyst supported on Al_2O_3

and Al_2O_3 -MgO was attributed to the octahedral species of Molybdenum, that seems to be a dominant specie in the monolayer due to molybdenum and oxygen polymeric in octahedral coordination; this band was not observed in the catalyst that contains lithium, which shows another band located at 903 cm^{-1} that is attributed to the tetrahedral species of Mo; it is important to remark that band located in 903 cm^{-1} is not observed in catalyst supported on Al_2O_3 and Al_2O_3 -MgO. It seems that lithium incorporation promotes that the band at 964 cm^{-1} attributed to the octahedral Mo species disappear and the band located at 903 cm^{-1} assigned to tetrahedral species appear, all this changes are related to the Mo(T)/Mo(O) increased ratio,which is accord to the observed in Kubelka Munk spectra and also is according to the reported before in a previous work in similar catalytic formulations that no contain tungsten. From this analysis is corroborated that the Raman results are in concordance with the observed by XRD.

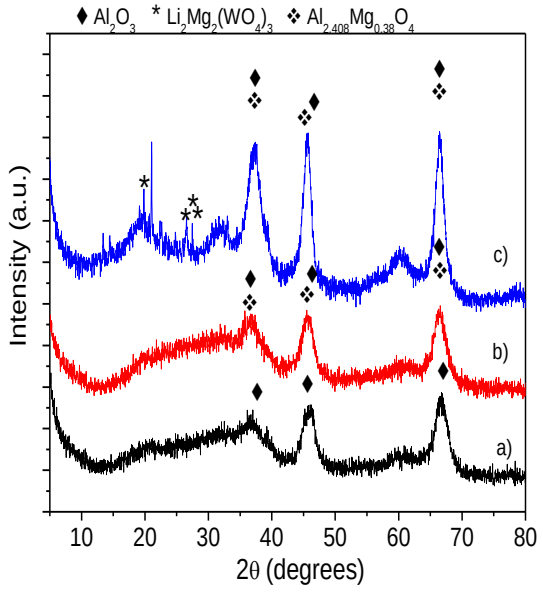

JCPDS	Crystalline phases
01-074-2206	♦ γ-Al_2O_3
00-048-0528	❖ $Al_{2.408}Mg_{0.38}O_4$
01-082-1804	* $Li_2Mg_2(WO_4)_3$

Fig. 3. X-ray diffraction of a) CoMoW/Al_2O_3, b) CoMoW/Al_2O_3-MgO and c) CoMoW/Al_2O_3-MgO—Li_2O.

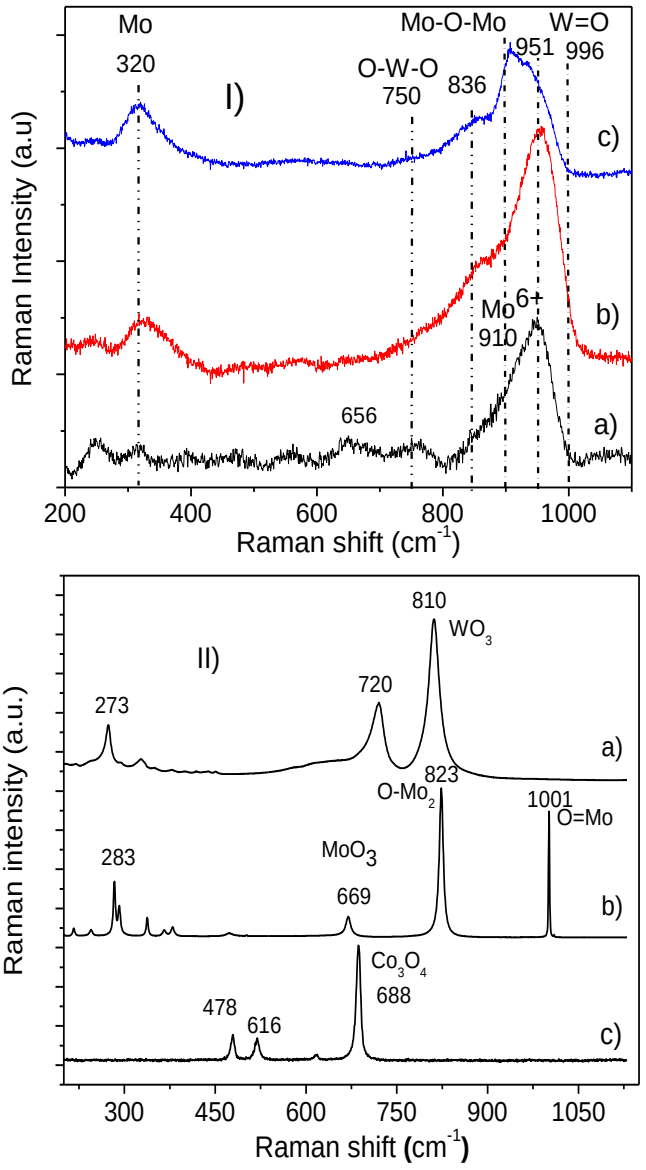

Fig. 4. Raman spectra of catalysts, I), a) CoMoW/Al_2O_3, b) CoMoW/Al_2O_3-MgO c) CoMoW/Al_2O_3-MgO-Li_2O and II) Masic unsupported a) WO_3, b) MoO_3 and c) Co_3O_4.

Diffuse reflectance spectroscopy measurements were performed to gain insight about the electronic transitions and coordination of the Mo, W and Co species when are supported on alumina modified with magnesia and lithia. Figure 5 shows the UV-Vis spectra in the diffuse reflectance mode (DRS), recorded in the range from 200 to 800 nm, for the different CoMoW catalysts. The wide band below 350 nm reveals the presence of two peaks at around 233–250 nm attributed to the tungsten and molybdena tetrahedral bands respectively. The signal around 262–300 nm is attributed to the octahedral species of tungsten and molybdenum (Radwan, Turky, & El-Shobaky, 2002).

In order to perform a deeper analysis, the DRS spectra were deconvoluted using gaussians as fitting functions. Integrated areas of deconvoluted peaks can be used to estimate the tetrahedral/octahedral Mo and W ratios. It is important to remark that this ratio increases with lithium incorporation to the catalytic formulation, suggesting that Li favors a change from octahedral to tetrahedral species in good agreement with the Raman analysis.

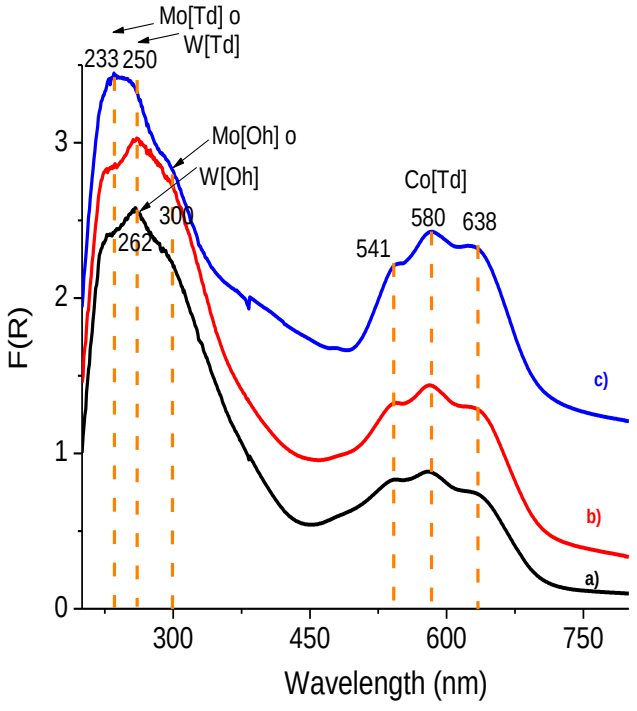

Fig. 5. Function of kubelka munk obtained by diffuse reflectance, for catalysts a) CoMoW/Al_2O_3, b) CoMoW/Al_2O_3-MgO and c) CoMoW/Al_2O_3-MgO-Li_2O.

Additionally, DRS spectra show a broad band al longer wavelengths, composed for at least three signals peaking at 541, 580 and 638 nm, characteristic signals of supported cobalt with tetrahedral symmetry ($CoAl_2O_4$) indicatives of the interaction between Co and the support suggesting the formation of a new compound (Mendoza-Nieto, Vera-Vallejo, Escobar-Alarcón, Solís-Casados, & Klimova, 2013). The DRS spectra of each CoMoW catalyst were treated using the Kubelka-Munk method to obtain the absorption edges and to determine the optical band gap energy, considering a direct band gap energy with allowed transitions as was reported by Weber (1995). It was assumed that this value is related with particle aggregation through the near neighbor's correlations. Figure 6.I) shows a red shift of the absorption edge of the polyoxomolybdates supported on Al_2O_3, Al_2O_3-MgO, Al_2O_3-MgO-Li_2O respect to the unsupported MoO_3. It is clear that unsupported MoO_3 shows the lowest band gap energy, 3.0 eV, due to its high agglomeration; when molybdenum is supported on Al_2O_3, Al_2O_3-MgO, Al_2O_3-MgO-Li_2O higher band gap energies are found, 3.5, 3.4 and 3.6 eV, respectively, suggesting that support containing magnesium and lithium favors the molybdenum species dispersion. Figure 6.II) shows the absorption edges of tungstates supported on Al_2O_3, Al_2O_3-MgO, Al_2O_3-MgO-Li_2O respect to the unsupported WO_3; WO_3 has a band gap energy of 2.7 eV due to its high agglomeration and when is supported on Al_2O_3, Al_2O_3-MgO, Al_2O_3-MgO-Li_2O the band gap energy increases from to values 4.2, 4.3 and 4.4 eV respectively; again, this is indicative of the good dispersion of W due to the modification of the catalytic support. In the case of cobalt, the effect of agglomeration on the band gap energy is less evident, the Co_3O_4 has a small value of 1.4 eV, whereas the cobalt impregnated on Al_2O_3 support shifts to 1.5 eV, and for the Co supported on Al_2O_3-MgO and Al_2O_3-MgO-Li_2O the corresponding values are 1.8 and 1.7 eV as it is seen in figure 6. III). The CoMoW impregnated on Al_2O_3-MgO-Li_2O have a slight shift in the absorption edge to 3.6 eV figure 6. IV), which indicates a good dispersion of the catalytic active phases in this support, that could be most related to the impregnating solution containing metallic citrates to enhance metallic dispersion. The absorption edges of these metal oxides show that larger aggregates have the lower energies as in (Weber, 1995). This band gap energy values indicate the good dispersion of the octahedral Mo and W species towards the tetrahedral species, which is in agreement with the dispersion suggested by the XRD and Raman results.

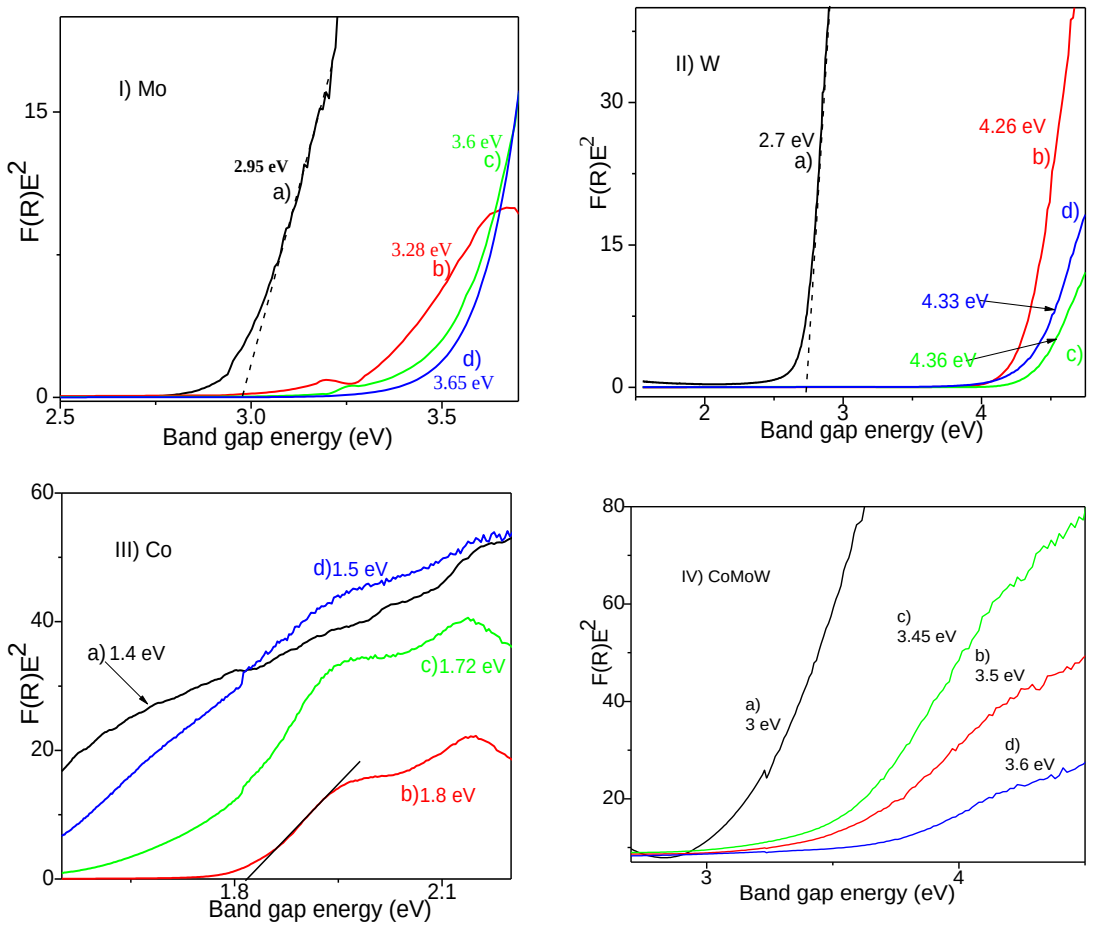

Fig. 6. I) Band gap energy for Mo catalysts a) unsupported MoO_3 and supported on b) Al_2O_3, c) Al_2O_3-MgO and d) Al_2O_3-MgO-Li_2O. II) Band gap energy for W catalysts a) unsupported WO_3 and supported on b) Al_2O_3, c) Al_2O_3-MgO and d) Al_2O_3-MgO-Li_2O. III) Band gap energy for Co catalysts a) unsupported Co_3O_4 and supported on b) Al_2O_3, c) Al_2O_3-MgO and d)Al_2O_3-MgO-Li_2O. IV) Band gap energy for CoMoW catalysts a) unsupported and supported on b) Al_2O_3, c) Al_2O_3-MgO and d) Al_2O_3-MgO-Li_2O.

3.2 CATALYTIC TESTS

Once catalytic formulations were characterized, their catalytic activity was evaluated through the HDS reaction of DBT molecule. In figure 7 I) it is observed the kinetic reaction constants determined assuming a pseudo-first order reaction. It is important to emphasize that Mg incorporation increases in 47 % the catalytic activity determined through the kinetic reaction constant; however, Li incorporation decreases the catalytic activity with a similar activity as in the Al_2O_3 supported catalyst. Regarding selectivity, figure 7 II) shows that for the CoMoW/Al_2O_3 catalysts the main reaction product is the biphenyl (BP) which is obtained from the direct desulphurization route, with the reaction time the biphenyl is hydrogenated to cyclohexylbenzene (CHB). This demonstrate that this formulation has a higher hydrogenation function probably due to the presence of W (Halatchev, Atanasova, Agudo, Arias, & Ramirez, 1996; Payen et al., 1994). Typically, the BP is not hydrogenated to CHB if DBTis present in the reaction medium, reaching the saturation when the dibenzothiophene is consumed (close to 100 % conversion) (Halatchev et al., 1996; Payen et al., 1994; Solís-Casados, Klimova, Ramírez, & Cortez 2004). In the present case, upon reaching conversion greater than 50 %, the selectivity to CHB begins to decrease as starts the formation of bicyclohexyl due to the saturating properties of the catalysts. Regard to the catalyst CoMoW supported on Al_2O_3-MgO (figure 7 III)), it is observed that the main product is BP. The selectivity to CHB decreases and the BCH is not detected, probably because BCH rapidly cracks to lighter products. However, at a DBT conversion close to 80% the BP is quickly

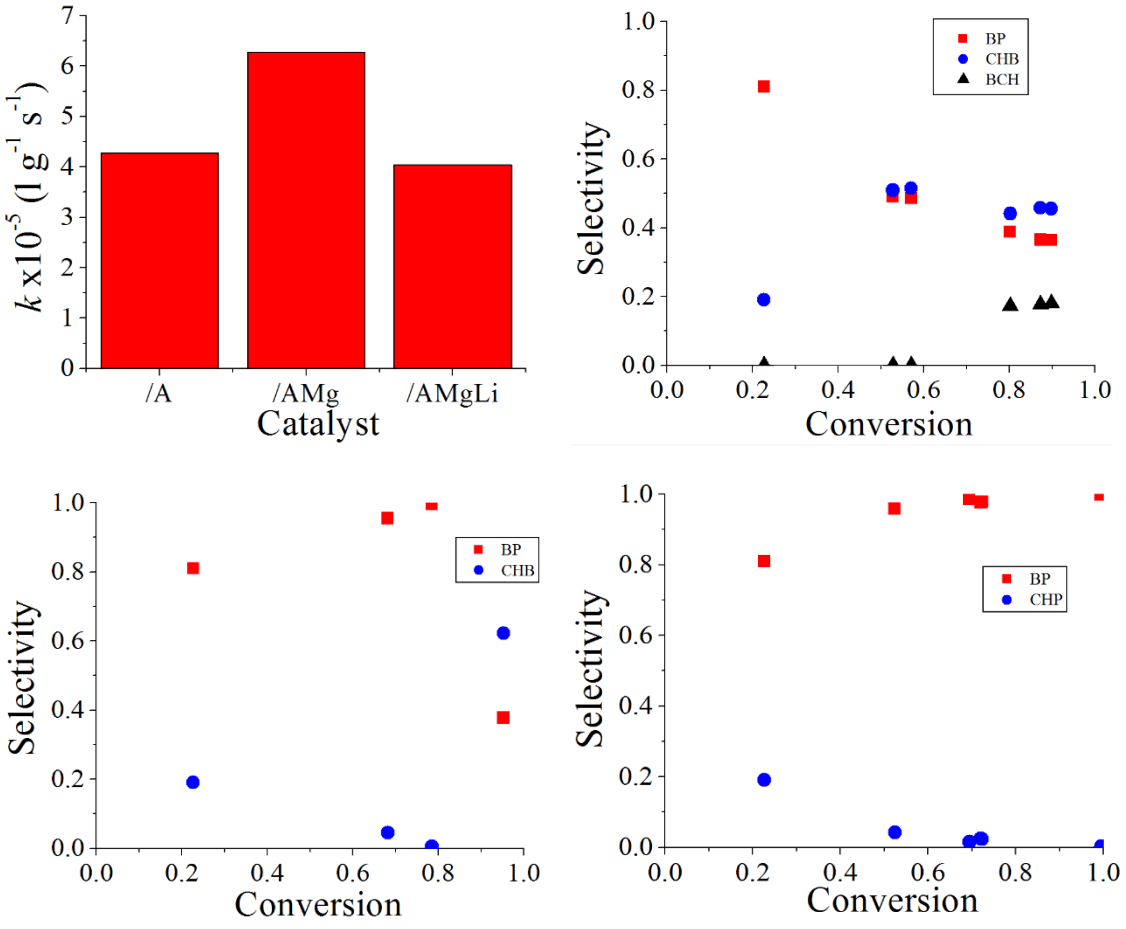

Fig. 7. I. Kinetic reaction constant of pseudo-first order for the CoMoW supported on a) Al_2O_3, b) Al_2O_3-MgO and c) Al_2O_3-MgO-Li_2O; II) Selectivity in HDS of DBT obtained with CoMoW/Al_2O_3. III) Selectivity in HDS of DBT obtained with CoMoW/Al_2O_3-MgO. Selectivity in HDS of DBT obtained with CoMoW/Al_2O_3-MgO-Li_2O.

hydrogenated to CHB, so the selectivity to the latter clearly increases. Finally, the catalyst containing Mg and Li (figure 7 IV)) seems to show lower saturating properties amongst the three formulations tested, since the BP does not saturate to CHB as occur in the previous cases.

4. CONCLUSIONS

CoMoW supported on Al_2O_3, Al_2O_3-MgO, Al_2O_3-MgO-Li_2O with lower number of acid sites and reduced acidic strength were prepared successfully. The CoMoW active phases were well dispersed in the three supports nevertheless of the high deposited metallic charge as XRD, Raman and DRS results reveal. An increase in the catalytic activity was observed in the HDS of DBT with Mg incorporation to the catalytic formulation. The simultaneous incorporation of Mg and Li into the formulation produce the same catalytic activity as the observed for the CoMoW/Al_2O_3 catalyst. However, it is important to emphasize that the formulation containing Mg and Li shows a better selectivity towards direct desulphurization, which is attributed to the decrease in acidity and acidic strength as well as to the good metallic dispersion obtained, due to the presence Mg and Li in support.

ACKNOWLEDGEMENTS

Authors thank to the UAEM 4488 project. Authors also thank to Dr. Uvaldo Hernández B. for the X-ray diffraction measurements, Dra. Susana Hernández by the TGA-DSC data, to M en C Alejandra Núñez, M en C Lizbeth Triana, Dra. Melina Tapia and LIA Citlalit Martinez for their technical support.

CONFLICT OF INTERESTS

The authors declare that they do not have conflict of interests.

REFERENCES

Clark R.J.H. and Hester R.E. (1987). Spectroscopy of inorganic materials. Advances in spectroscopy 14, 187.

Escobar-Alarcón, L., Klimova, T., Escobar-Aguilar, J., Romero, S., Morales-Ramírez, C., & Solís-Casados, D. (2013). Preparation and characterization of Al2O3–MgO catalytic supports modified with lithium. *Fuel*, *110*, 278-285.

Gómez-Orozco, S.Y., Huirache-Acuña, R., Pawelec, B., Fierro, J.L.G., Rivera-Muñoz, E.M., Lara-Romero, J., Alonso-Nuñez, G. (2018). Characterizations and HDS performances of sulfided NiMoW catalysts supported on mesoporous titania-modified SBA-15 Catalysis Today 305, 152-161.

Halachev, T., Atanasova, P., Agudo, A. L., Arias, M. G., & Ramirez, J. (1996). Activity of P-Ni-W/Al2O3 catalysts with varying phosphorus content in the hydrogenation of naphthalene. *Applied Catalysis A: General*, *136*(2), 161-175.

Huirache-Acuña, R., Albiter, M. A., Paraguay-Delgado, F., Lumbreras Pacheco, J. A., Ornelas, C., Martínez-Sanchez, R., & Alonso-Nunez, G. (2006). Síntesis y caracterización de catalizadores no soportados de sulfuros de Ni, Mo y W para la HDS de DBT. *Revista Mexicana de Ingeniería Química*, *5*(3), 285-292.

Klicpera, T., & Zdražil, M. (2002). Preparation of high-activity MgO-supported Co–Mo and Ni–Mo sulfide hydrodesulfurization catalysts. *Journal of Catalysis*, *206*(2), 314-320.

Klimova, T., Casados, D. S., & Ramírez, J. (1998). New selective Mo and NiMo HDS catalysts supported on Al2O3–MgO (x) mixed oxides. *Catalysis Today*, *43*(1-2), 135-146.

Kwak, C., Lee, J. J., Bae, J. S., Choi, K., & Moon, S. H. (2000). Hydrodesulfurization of DBT, 4-MDBT, and 4, 6-DMDBT on fluorinated CoMoS/Al2O3 catalysts. *Applied Catalysis A: General*, *200*(1-2), 233-242.

Mendoza-Nieto, J. A., Vera-Vallejo, O., Escobar-Alarcón, L., Solís-Casados, D., & Klimova, T. (2013). Development of new trimetallic NiMoW catalysts supported on SBA-15 for deep hydrodesulfurization. *Fuel*, *110*, 268-277.

Nikulshina, M., Mozhaev, A., Lancelot, C., Blanchard, P., Marinova, M., Lamonier, C., & Nikulshin, P. (2019). Enhancing the hydrodesulfurization of 4, 6-dimethyldibenzothiophene through the use of mixed MoWS2 phase evidenced by HAADF. *Catalysis Today*, *329*, 24-34.

Obeso-Estrella, R., Fierro, J.L. G. de León, J.N. D., Fuentes, S., Alonso-Nuñez, G., Lugo-Medina, E., Pawelec, B., Zepeda, T.A. (2018). Effect of partial Mo substitution by W on HDS activity using sulfide CoMoW /Al2O3-TiO2 catalysts. fuel 233, 644-657.

Payen, E., Hubaut, R., Kasztelan, S., Poulet, O., & Grimblot, J. (1994). Morphology study of MoS2-and WS2-based hydrotreating catalysts by high-resolution electron microscopy. *Journal of Catalysis*, *147*(1), 123-132.

Pérez-Martínez, D. J., Eloy, P., Gaigneaux, E. M., Giraldo, S. A., & Centeno, A. (2010). Study of the selectivity in FCC naphtha hydrotreating by modifying the acid–base balance of CoMo/γ-Al2O3 catalysts. Applied Catalysis A: General, 390(1-2), 59-70.

Radwan, N.R.E, Turky, A.E.-M.M., El-Shobaky, G.A. (2002). Surface and catalytic properties of Co3O4/Al2O3 as influenced by ZnO. Colloids and Surfaces A: Physicochemical and Engineering Aspects, 203(1-3), 87-95.

Rinaldi N., Kubota T., Okamoto Y. (2010) Appl. Catal. A: Gen. 374, 228.

Ganiyu, S. A., Ali, S. A., & Alhooshani, K. (2017). Simultaneous HDS of DBT and 4, 6-DMDBT over single-pot Ti-SBA-15-NiMo catalysts: influence of Si/Ti ratio on the structural properties, dispersion and catalytic activity. RSC Advances, 7(35), 21943-21952.

Wang, S., Wang, R., & Yu, H. (2012). Deep removal of 4, 6-dimethyldibenzothiophene from model transportation diesel fuels over reactive adsorbent. Brazilian Journal of Chemical Engineering, 29(2), 421-428.

Ding, S., Zhou, Y., Wei, Q., Jiang, S., & Zhou, W. (2018). Substituent effects of 4, 6-DMDBT on direct hydrodesulfurization routes catalyzed by Ni-Mo-S active nanocluster—A theoretical study. Catalysis Today, 305, 28-39.

Solís-Casados, D., Escobar, J., Orozco, I. G., & Klimova, T. (2010). Effect of potassium content on the performance of CoMo/Al2O3-MgO-K2O (x) catalysts in hydrodesulfurization of dibenzothiophene. Industrial & Engineering Chemistry Research, 50(5), 2755-2761.

Solís-Casados, D. A., Escobar-Alarcón, L., Klimova, T., Escobar-Aguilar, J., Rodríguez-Castellón, E., Cecilia, J. A., & Morales-Ramírez, C. (2016). Catalytic performance of CoMo/Al2O3-MgO-Li (x) formulations in DBT hydrodesulfurization. Catalysis Today, 271, 35-44.

Solis, D., Klimova, T., Ramírez, J., & Cortez, T. (2004). NiMo/Al2O3–MgO (x) catalysts: the effect of the prolonged exposure to ambient air on the textural and catalytic properties. Catalysis today, 98(1-2), 99-108.

Vakros, J., Lycourghiotis, A., Voyiatzis, G. A., Siokou, A., & Kordulis, C. (2010). CoMo/Al2O3-SiO2 catalysts prepared by co-equilibrium deposition filtration: Characterization and catalytic behavior for the hydrodesulphurization of thiophene. Applied Catalysis B: Environmental, 96(3-4), 496-507.

Weber, R. S. (1995). Effect of local structure on the UV-visible absorption edges of molybdenum oxide clusters and supported molybdenum oxides. Journal of Catalysis, 151(2), 470-474.